# Scattering and diffraction of plane *SH*-waves by two-dimensional inhomogeneities: Part I

Nasser Moeen-Vaziri and Mihailo D. Trifunac

Dept. of Civil Engineering, University of Southern California, University Park, Los Angeles, CA 90089-1114, USA

A wave expansion technique is presented for the analysis of scattered and diffracted plane *SH*-waves by two-dimensional inhomogeneities. Comparison of this approximate method with exact series solutions suggests that the proposed method may become a useful tool in predicting the local site amplification patterns in earthquake engineering applications which deal with the estimation of site specific spectra and in the problems involving earthquake response of long structures with multiple supports.

## INTRODUCTION

The local ground amplification effects caused by surface and subsurface irregularities represent an important factor which modifies the recorded surface motions during strong earthquake shaking. Detailed understanding of these effects is of obvious value to earthquake engineering and strong motion seismology. In reviewing the methods of analysis in this subject area (Moen-Vaziri and Trifunac[1]), one finds discrete and continuous methods of solution. The discrete methods include finite elements and finite differences. Due to large dimensions in geophysical problems, the application of such discrete methods may be limited. On the other hand, the applicability of continuous methods is restricted to linear, isotropic and homogeneous materials and to simple geometries.

There has been a considerable amount of work done on elastic *SH*-wave scattering problems using continuous methods. Trifunac[2] analysed scattering of plane *SH*-waves by a semi-cylindrical canyon using an exact solution. Sabina and Willis[3] used the method of asymptotoc expansions to investigate the effects of topographic irregularities in scattering of plane *SH*-waves. England *et al.*[4] solved the problem of scattering of *SH*-waves by a bounded cavity of arbitrary shape in a half-space by minimizing the mean-square error in the boundary conditions on the cavity. Sills[5] considered the scattering problem of harmonic *SH*-waves by arbitrary surface irregularities. An exact series solution was presented by Wong and Trifunac[6] to examine surface amplifications due to scattering of plane *SH*-waves by a semi-elliptical canyon. Sanchez-Sesma and Rosenblueth[7] studied scattering of *SH*-waves by canyons of arbitrary shape. A comparison of experimental and analytical results for the effects of surface and subsurface irregularities on ground motion was carried out by Wong *et al.*[8]. According to their study ground motion is more influenced by the shallow alluvium layer than by the canyon. Sanchez-Sesma *et al.*[9] presented a boundary method to investigate the scattering and diffraction of

*SH*-waves by surface irregularities. They used a least-squares technique to satisfy the boundary conditions. The problem of scattering and diffraction of *SH*-waves by irregular canyon topography was also studied by Wong and Jennings[10] in terms of an integral equation.

The models with different material properties in elastic wave scattering and diffraction have been analysed as well. Trifunac[11] investigated the surface motion in and around a semi-cylindrical alluvial valley excited by plane *SH*-waves, using an exact series solution. Wong and Trifunac[12] extended this type of analytical solution in terms of Mathieu functions to obtain the surface motion of a semi-elliptical alluvial valley due to *SH*-wave excitation. Aki and Larner[13] devised a method to calculate the surface motion of a layer over half-space medium with small interface irregularities. Bard and Bouchon[14] studied the seismic response of sediment filled valleys for incident *SH*-waves by presenting an extension to time domain calculations of Aki and Larner[13]. The ground motion due to scattering and diffraction of *SH*-waves by an arbitrary shaped alluvial valley was studied by Sanchez-Sesma and Esquivel[15]. They used a least-squares procedure to satisfy the boundary conditions. Lee and Trifunac[16] studied stresses and deformations near circular underground tunnels subjected to incident *SH*-waves. The surface displacement and stress amplitudes of a semi-circular canal bounded in an elastic half-space, excited by plane *SH*-waves, were studied by Moeen-Vaziri and Trifunac[17]. Moeen-Vaziri and Trifunac[18] used a boundary method to solve numerically the problem of scattering and diffraction of *SH*-waves by cylindrical canals of arbitrary shape in an elastic half-space.

The objective of this study is to summarize the work of Moeen-Vaziri and Trifunac[1] on the effects of subsurface inhomogeneities and irregularities of arbitrary shape on the ground motion amplification. The numerical applications made in this presentation centre around *SH* waves. The method of analysis used in this work represents an extension of the work done by Sanchez-Sesma[19], on diffraction of elastic waves by three dimensional surface irregularities, and by Moeen-Vaziri and Trifunac[18], on scattering of plane *SH*-waves by cylindrical canals of arbitrary shape.

## 1.1 Wave equation in polar coordinates

For the model considered in this, work the polar coordinate system is suitable for use. Let the function $f$ be of the form $f = f(r, \theta, t)$. The wave equation

$$c^2 \nabla^2 f - \frac{\partial^2 f}{\partial t^2} = 0 \qquad (1.2.1)$$

in polar coordinates is then

$$\frac{\partial^2 f}{\partial r^2} + \frac{1}{r} \frac{\partial f}{\partial r} + \frac{1}{r^2} \frac{\partial^2 f}{\partial \theta^2} = \frac{1}{c^2} \frac{\partial^2 f}{\partial t^2} \qquad (1.2.2)$$

where $c$ is the wave velocity.

Since the arbitrary time variation of the function can be represented by Fourier analysis in terms of harmonic functions, there will be no loss of generality in considering only the harmonic solution of the form

$$f(r, \theta, t) = F(r, \theta) e^{i\omega t} \qquad (1.2.3)$$

where $i = \sqrt{-1}$, $\omega$ is the circular frequency and $F$ satisfies the Helmholtz equation

$$\nabla^2 F + K^2 F = 0 \qquad (1.2.4)$$

in which $K = \omega/c$ is the wave number.

By using the method of separation of variables with $F = R(r)\Theta(\theta)$ equation (1.2.4) separates into

$$r^2 R'' + rR' + (K^2 r^2 - p^2)R = 0 \qquad (1.2.5)$$

$$\Theta'' + p^2 \Theta = 0 \qquad (1.2.6)$$

where $p$ is the separation constant. The solutions for $\Theta(\theta)$ are

$$\Theta = e^{\pm ip\theta} \quad \text{or} \quad \begin{pmatrix} \sin p\theta \\ \cos p\theta \end{pmatrix} \qquad (1.2.7)$$

For most problems of interest, $\Theta$ must be single valued, i.e., $\Theta(\theta + 2\pi) = \Theta(\theta)$, which requires $p = n$, where $n$ in an integer. Equation (1.2.5) then becomes

$$r^2 R'' + rR' + (K^2 r^2 - n^2)R = 0 \qquad (1.2.8)$$

with the solution than can be expressed in terms of either Bessel functions of the first and second kind, $J_n(Kr)$ and $Y_n(Kr)$ respectively, or in terms of Hankel functions of the first and second kind, $H_n^{(1)}(Kr)$ and $H_n^{(2)}(Kr)$.

Therefore, let the general solution of equation (1.2.8) be of the form $X_n^{(m)}(Kr)$, $m = 1,2,3,4$, defined as follows:

$$X_n^{(1)} = J_n(Kr)$$

$$X_n^{(2)} = Y_n(Kr)$$

$$X_n^{(3)} = H_n^{(1)}(Kr)$$

$$X_n^{(4)} = H_n^{(2)}(Kr) \qquad (1.2.9)$$

Then the general solution of the wave equation (1.2.2) is any linear combination of two of

$$X_n^{(m)}(Kr) \frac{\sin n\theta}{\cos n\theta} \exp(i\omega t) \qquad (1.2.10)$$

with $m = 1, 2, 3, 4$, and $n = 0, 1, 2, \ldots$.

The two dimensional model studied in this work is shown in Fig. 1. It represents a layered half space $(y > 0)$ with each layer having arbitrary shape. The soil and
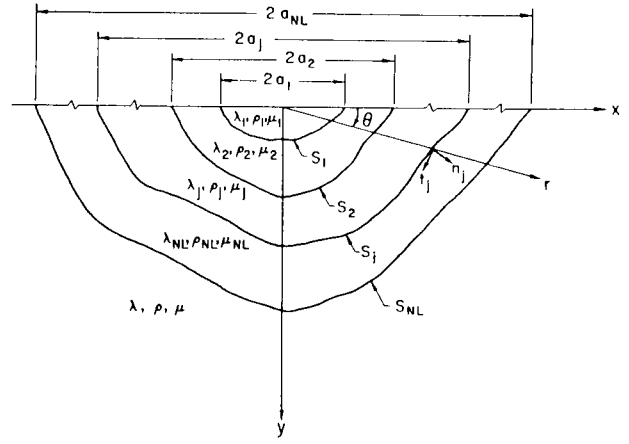


*Fig. 1. The Model*

alluvium are assumed to be elastic and linear, and the contact between the layers is assumed to be welded. The material property of the $j$th layer is given by Lamé constants $\lambda_j$ and $\mu_j$, and mass density $\rho_j$, $j = 1, 2, 3, \ldots$, $NL$, for which we have

longitudinal wave velocity: $\alpha_j = \sqrt{\dfrac{\lambda_j + 2\mu_j}{\rho_j}}$

and

transverse wave velocity: $\beta_j = \sqrt{\dfrac{\mu_j}{\rho_j}} \qquad (1.2.11)$

$NL$ is the total number of layers. The characteristic horizontal linear dimension of each layer is defined by $2a_j$, $j = 1, 2, 2, 3, \ldots, NL$.

Three coordinate systems are introduced. The rectangular coordinate system with positive $x$ pointing to the right and positive $y$ pointing down. The cylindrical coordinate system, consisting of the radial distance $r$ and the angle $\theta$, measured from the positive $x$ coordinate has a common origin with the rectangular system. Finally, the normal-tangential local coordinate system $(n_j, t_j)$, is employed which consists of the outward normal $n_j$ to the outer boundary of layer $j$, $j = 1, 2, \ldots, NL$, and the tangent to this boundary $t_j$ (Fig. 1).

## 2. EXCITATION: INCIDENT SH-WAVE

The excitation of the half-space, $u_z^i$, is assumed to consist of an infinite train of plane SH-waves with frequency '$\omega$' and particle motion in the $z$-direction as follows:

$$u_z^i = \exp i\omega \left( t - \frac{x}{C_{sx}} + \frac{y}{C_{sy}} \right) \qquad (2.1.1)$$

For an incident angle $\gamma$ the phase velocities along the $x$ axis, $C_{sx}$, and $y$ axis, $C_{sy}$, are given by (see Fig. 2)

$$C_{sx} = \frac{\beta}{\cos \gamma} \qquad C_{sy} = \frac{\beta}{\sin \gamma} \qquad (2.1.2)$$

in which $\beta$ is the shear wave velocity in the half-space.

Far from any inhomogeneities, the incident waves are reflected from the free surface $(y = 0)$ and in the free-field
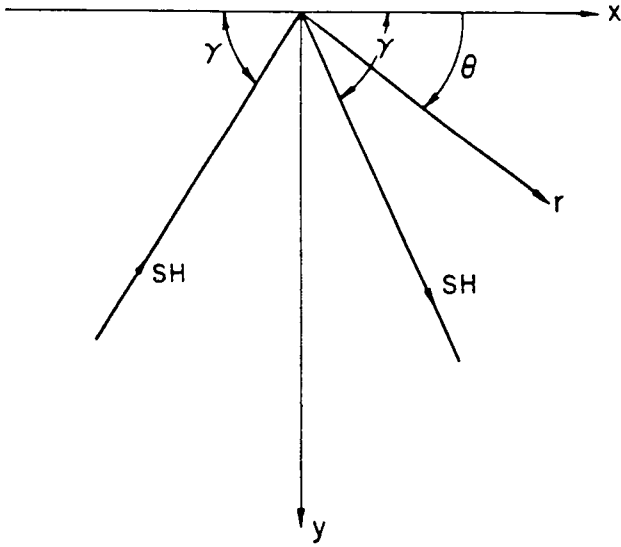
*Fig. 2. Incident SH-wave*

region incident $u_z^i$ and reflected $u_z^r$ waves interfere to give the resulting motion

$$u_z^{i+r} = u_z^i + u_z^r = 2\exp\left[i\omega\left(t - \frac{x}{C_{sx}}\right)\right]\cos\left(\frac{\omega y}{C_{sy}}\right) \qquad (2.1.3)$$

It is convenient to represent the excitation, equation (2.1.1), in terms of the functions of $r$ and $\theta$. It can be shown that with:

$$x = r\cos\theta \quad \text{and} \quad y = r\sin\theta$$

$$u_z^i = \exp i[\omega t - Kr\cos(\theta + \gamma)] \qquad (2.1.4)$$

It follows then that (Pao and Mow[20])

$$u_z^{i+r} = u_z^i + u_z^r$$

$$= 2\sum_{n=0}^{\infty} d_n(-i)^n J_n(Kr)\cos\theta\cos n\gamma\, e^{i\omega t}$$

$$(2.1.5)$$

where $J_p(x)$ are Bessel functions of the first kind with argument $x$ and order $p$, $K = \omega/\beta$ is shear wave number in the free-field region, and $d_n$ is defined as follows:

$$d_n = \begin{cases} 1 & \text{for } n = 0 \\ 2 & \text{for } n \geqslant 1 \end{cases}$$

From this point on, the time factor $\exp(i\omega t)$ will be understood and omitted from all expressions.

Close to an inhomogeneity, say a layer, incident $u_z^i$ and the waves $u_z^r$ reflected from the surface $y = 0$, are scattered and diffracted by the outer boundary of the layer, $S_{NL}$ (Fig. 1). The new group of scattered and diffracted waves is called $u_z^R$. The resultant free-field displacement $u_z^{ff}$, is then

$$u_z^{ff} = u_z^i + u_z^r + u_z^R \qquad (2.1.6)$$

The waves are also refracted into the inhomogeneity, a layer. These motions are denoted by $u_z^{fj}$, $j = 1, 2, 3, \ldots, NL$, for all layers, inside the inhomogeneity (Fig. 1).

## 2.1 Boundary conditions

The free-field motion $u_z^{ff}$ and the motion in each layer $u_z^{fj}, j = 1, 2, \ldots, NL$ must satisfy the differential equation (1.2.2) and the following boundary conditions:

(1) The stress free condition on the surface of the half-space

$$\sigma_{\theta z}^{f_1} = \frac{\mu_1}{r}\frac{\partial u_z^{f_1}}{\partial \theta} = 0 \qquad \begin{array}{l}\text{at } \theta = 0 \text{ and } \theta = \pi \text{ and } r \text{ in the} \\ \text{first layer}\end{array}$$

$$\sigma_{\theta z}^{f_2} = \frac{\mu_2}{r}\frac{\partial u_z^{f_2}}{\partial \theta} = 0 \qquad \begin{array}{l}\text{at } \theta = 0 \text{ and } \theta = \pi \text{ and } r \text{ in the} \\ \text{second layer} \qquad\qquad (2.2.1)\end{array}$$

$$\vdots \qquad\qquad \vdots$$

$$\sigma_{\theta z}^{f_{NL}} = \frac{\mu_{NL}}{r}\frac{\partial u_z^{f_{NL}}}{\partial \theta} = 0 \qquad \begin{array}{l}\text{at } \theta = 0 \text{ and } \theta = \pi \text{ and } r \text{ in the} \\ \text{last layer}\end{array}$$

$$\sigma_{\theta z}^{ff} = \frac{\mu}{r}\frac{\partial u_z^{ff}}{\partial \theta} = 0 \qquad \begin{array}{l}\text{at } \theta = 0 \text{ and } \theta = \pi \text{ and } r \text{ in the} \\ \text{half-space} \qquad\qquad (2.2.2)\end{array}$$

(2) Continuity of displacements

$$u_z^{f_1} = u_z^{f_2} \qquad \text{on } S_1$$

$$u_z^{f_2} = u_z^{f_3} \qquad \text{on } S_2 \qquad (2.2.3)$$

$$\vdots$$

$$u_z^{f_{NL-1}} = u_z^{f_{NL}} \qquad \text{on } S_{NL-1}$$

$$u_z^{f_{NL}} = u_z^{ff} \qquad \text{on } S_{NL} \qquad (2.2.4)$$

and (3) Continuity of stress

$$\mu_1\frac{\partial u_z^{f_1}}{\partial \hat{n}_1} = \mu_2\frac{\partial u_z^{f_2}}{\partial \hat{n}_1} \qquad\qquad \text{on } S_1$$

$$\mu_2\frac{\partial u_z^{f_2}}{\partial \hat{n}_2} = \mu_3\frac{\partial u_z^{f_3}}{\partial \hat{n}_2} \qquad\qquad \text{on } S_2 \qquad (2.2.5)$$

$$\vdots \qquad\qquad \vdots$$

$$\mu_{NL-1}\frac{\partial u_z^{f_{NL-1}}}{\partial \hat{n}_{NL-1}} = \mu_{NL}\frac{\partial u_z^{f_{NL}}}{\partial \hat{n}_{NL-1}} \qquad \text{on } S_{NL-1}$$

$$\mu_{NL}\frac{\partial u_z^{f_{NL}}}{\partial \hat{n}_{NL}} = \mu\frac{\partial u_z^{ff}}{\partial \hat{n}_{NL}} \qquad\qquad \text{on } S_{NL} \qquad (2.2.6)$$

$2a_j$ is the total width of the $j$th layer and $\hat{n}_j$ is the unit normal to $s_j$, the outer boundary of each layer for $j = 1, 2, \ldots, NL$ (Fig. 1). The derivative in the direction of this unit normal is denoted by $\partial/\partial\hat{n}_j$. Furthermore, $u_z^{ff}$ must satisfy the Sommerfeld's outward radiation conditions at infinity.

Once $u_z^R$ and $u_z^{fj}, j = 1, 2, \ldots, NL$ are found, the free-field displacement and the displacement in each layer can be determined.

## 2.2 Solution of the problem

Consider the following sets of linearly independent functions:

$$_jQ_n^{(1)}(\mathbf{x}) \qquad _jQ_n^{(2)}(\mathbf{x}) \qquad \begin{array}{l}n = 0, 1, 2, 3, \ldots \\ j = 1, 2, \ldots, NL\end{array} \qquad (2.3.1)$$

and

$$P_n(\mathbf{x}) \qquad n = 0, 1, 2, 3, \ldots \qquad (2.3.2)$$

which are not necessarily orthogonal, and have the following properties:

(i) Each $P_n$ is a solution of the partial differential equation (1.2.2) in the free-field region and $_jQ_n^{(1)}$ and $_jQ_n^{(2)}$ are solutions of the same differential equation in the $j$th layer, with $C = \beta$ in (1.2.2).

(ii) $P_n$, $_jQ_n^{(1)}$ and $_jQ_n^{(2)}$ satisfy:

$$\frac{\partial P_n}{\partial \hat{n}_{NL}} = 0 \quad \frac{\partial _jQ_n^{(1)}}{\partial \hat{n}_j} = 0 \quad \frac{\partial _jQ_n^{(2)}}{\partial \hat{n}_j} = 0 \quad \begin{array}{l} \text{on } y = 0 \\ j = 1, 2, \ldots, NL \end{array}$$

$$(2.3.3)$$

(iii) $P_n$ satisfies the Sommerfeld's outward radiation condition at infinity.

Next one can assume that:

$$u_z^{f_1} = \sum_{n=0}^{N} \left[ _1a_{n1}Q_n^{(1)}(\mathbf{x}) + _1b_{n1}Q_n^{(2)}(\mathbf{x}) \right]$$

$$u_z^{f_2} = \sum_{n=0}^{N} \left[ _2a_{n2}Q_n^{(1)}(\mathbf{x}) + _2b_{n2}Q_n^{(2)}(\mathbf{x}) \right] \qquad (2.3.4)$$

$$\vdots \qquad \qquad \vdots$$

and

$$u_z^{f_j} = \sum_{n=0}^{N} \left[ _ja_{nj}Q_n^{(1)}(\mathbf{x}) + _jb_{nj}Q_n^{(2)}(\mathbf{x}) \right]$$

$$u_z^{f_{NL}} = \sum_{n=0}^{N} \left[ _{NL}a_{nNL}Q_n^{(1)}(\mathbf{x}) + _{NL}b_{nNL}Q_n^{(2)}(\mathbf{x}) \right]$$

$$u_z^R = \sum_{n=0}^{N} c_n P_n(\mathbf{x}) \qquad (2.3.5)$$

Due to the linear character of the properties (i) through (iii), $u_z^R$ and $u_z^{f_j}$, $j = 1 2, \ldots, NL$, for $n = 0.1, 2, 3, \ldots, N$ also satisfy these properties. The waves (2.1.3) satisfy the boundary conditions (2.2.2). Therefore, the waves $u_z^{f_j}$ and $u_z^R$ must also satisfy the boundary conditions (2.2.1) and (2.2.2). Furthermore, the waves $u_z^{f_j}$ and $u_z^{f_f}$ must satisfy the boundary conditions listed in (2.2.3), (2.2.4), (2.2.5) and (2.2.6). By applying these conditions and by using equations (2.3.4) and (2.3.5), one can get the following equations in terms of the complex constants $a_n$, $b_n$ and $c_n$:

$$\sum_{n=0}^{N} {_1a_{n1}}Q_n^{(1)}(S_1^k) + \sum_{n=0}^{N} {_1b_{n1}}Q_n^{(2)}(S_1^k) - \sum_{n=0}^{N} {_2a_{n_2}}Q_n^{(1)}(S_1^k)$$

$$- \sum_{n=0}^{N} {_2b_{n_2}}Q_n^{(2)}(S_1^k) = 0 \qquad \text{on } S_1$$

$$\mu_1 \sum_{n=0}^{N} {_1a_n} \frac{\partial_1 Q_n^{(1)}(S_1^k)}{\partial \hat{n}_1} + \mu_1 \sum_{n=0}^{N} {_1b_n} \frac{\partial_1 Q_n^{(2)}(S_1^k)}{\partial \hat{n}_1}$$

$$- \mu_2 \sum_{n=0}^{N} {_2b_n} \frac{\partial_2 Q_n^{(1)}(S_1^k)}{\partial \hat{n}_1} - \mu_2 \sum_{n=0}^{N} {_2a_n} \frac{\partial_2 Q_n^{(2)}(S_1^k)}{\partial \hat{n}_1} = 0$$

$$\text{on } S_1$$

$$\sum_{n=0}^{N} {_2a_{n_2}}Q_n^{(1)}(S_2^k) + \sum_{n=0}^{N} {_2b_{n_2}}Q_n^{(2)}(S_2^k) - \sum_{n=0}^{N} {_3}Q_n^{(1)}(S_2^k)$$

$$- \sum_{n=0}^{N} {_3b_{n_3}}Q_n^{(2)}(S_2^k) = 0 \qquad \text{on } S_2$$

$$\mu_2 \sum_{n=0}^{N} {_2a_n} \frac{\partial_2 Q_n^{(1)}(S_2^k)}{\partial \hat{n}_2} + \mu_2 \sum_{n=0}^{N} {_3a_n} \frac{\partial_2 Q_n^{(2)}(S_2^k)}{\partial \hat{n}_2}$$

$$- \mu_3 \sum_{n=0}^{N} {_3a_n} \frac{\partial_3 Q_n^{(1)}(S_2^k)}{\partial \hat{n}_2} - \mu_3 \sum_{n=0}^{N} {_3b_n} \frac{\partial_3 Q_n^{(2)}(S_2^k)}{\partial \hat{n}_2} = 0$$

$$\text{on } S_2 \qquad (2.3.6)$$

$$\vdots$$

$$\sum_{n=0}^{N} {_ja_{n_j}}Q_n^{(1)}(S_j^k) + \sum_{n=0}^{N} {_jb_{n_j}}Q_n^{(2)}(S_j^k) - \sum_{n=0}^{N} {_{j+1}a_{n_{j+1}}}Q_n^{(1)}(S_j^k k)$$

$$- \sum_{n=0}^{N} {_{j+1}b_{n_{j+1}}}Q_n^{(1)}(S_2^k) = 0 \qquad \text{on } S_j$$

$$\mu_j \sum_{n=0}^{N} {_ja_n} \frac{\partial_j Q_n^{(1)}(S_j^k)}{\partial \hat{n}_j} + \mu_j \sum_{n=0}^{N} {_jb_n} \frac{\partial_j Q_n^{(2)}(S_j^k)}{\partial \hat{n}_j}$$

$$- \mu_{j+1} \sum_{n=0}^{N} {_{j+1}a_n} \frac{\partial_{j+1} Q_n^{(1)}(S_j^k)}{\partial \hat{n}_j}$$

$$- \mu_{j+1} \sum_{n=0}^{N} {_{j+1}b_n} \frac{\partial_{j+1} Q_n^{(2)}(S_j^k)}{\partial \hat{n}_j} = 0 \qquad \text{on } S_j$$

$$\sum_{n=0}^{N} {_{NL}a_{n_{NL}}}Q_n^{(1)}(S_{NL}^k) + \sum_{n=0}^{N} {_{NL}b_{n_{NL}}}Q_n^{(2)}(S_{NL}^k)$$

$$- \sum_{n=0}^{N} c_n P_n(S_{NL}^k) = u_z^{i+r}(S_{NL}^k) \qquad \text{on } S_{NL}$$

$$\mu_{NL} \sum_{n=0}^{N} {_{NL}a_n} \frac{\partial_{NL} Q_n^{(1)}(S_{NL}^k)}{\partial \hat{n}_{NL}} + \mu_{NL} \sum_{n=0}^{N} {_{NL}b_n} \frac{\partial_{NL} Q_n^{(2)}(S_{NL}^k)}{\partial \hat{n}_{NL}}$$

$$- \mu \sum_{n=0}^{N} C_n \frac{\partial P_n(S_{NL}^k)}{\hat{n}_{NL}} = \mu \frac{\partial u_z^{i+r}(S_{NL}^k)}{\partial \hat{n}_{NL}} \qquad \text{on } S_{NL}$$

In the above equations $j = 1, 2, \ldots, NL$, is the number of the layers used, and $k = 1, 2, 3, \ldots, M$, is the number of the points employed to apply the boundary conditions on each boundary. $S_j^k$ represents the argument of the functions at point $k$ and on the outer boundary of the $j$th layer.

The system of linear equations formed by equations (2.3.6) can be written as:

$$[A]\{C\} = \{F\} \qquad (2.3.7)$$

in which $[A]$ is the coefficient matrix, $\{C\}$ is the vector of complex constants $a_n$, $b_n$ and $c_n$, and $\{F\}$ is the vector formed by the right hand side of equations (2.3.6). The row dimension of $[A]$, $q$, is two times the number of the layers times the number of the points used on each boundary. The column dimension of $[A]$, $r$, is two times the number of the layers times the number of the terms used in each series. Vector $\{C\}$ has dimension $r \times 1$, while $\{F\}$ is a $q \times 1$ vector. For the problem considered in this work the system (2.3.7) is an overdetermined system, i.e. $q > r$. The solution $\{C\}$ that minimizes the mean square error on the boundary can be obtained by solving the

system (Moeen-Vaziri and Trifunac[1]):

$$[A*]^T[W][A]\{C\} = [A*]^T[W]\{F\} \qquad (2.3.8)$$

where $[A*]^T$ is the conjugate transpose of $[A]$, and $[W]$ is a diagonal matrix which contains the normalization factors. The resulting system of equations is of the order $r \times r$. Once the values of $a'_n$s, $b'_n$s and $c'_n$s are determined, the waves $u_z^{fj}$ and $u_z^{ff}$ are defined everywhere in the layers and in the free-field region.

So far the functions $_jQ_n^{(1)}(x)$, $_jQ_n^{(2)}(x)$ and $P_n(x)$ have been kept as general as possible. To proceed further, their detailed description is required. For the second layer through the last layer where both incoming and outgoing waves are present, one can consider the following sets of functions:

$$_jQ_n^{(1)} = H_n^{(1)}(K_jr)\cos n\theta$$

$$_jQ_n^{(2)} = H_n^{(2)}(K_jr)\cos n\theta \qquad j = 2, 3, \ldots, NL \qquad (2.3.9)$$

In the first layer the motion must have the finite amplitude at $r = 0$. For this layer the following can be assumed:

$$_1Q_n^{(1)} \equiv {}_1Q_n^{(2)} = J_n(K_1r)\cos n\theta \qquad (2.3.10)$$

For the outgoing motion in the free-field region one can assume

$$P_n = H_n^{(2)}(Kr)\cos n\theta \qquad (2.3.11)$$

In the above, $H_p^{(1)}(x)$ and $H_p^{(2)}(x)$ are the Hankel's functions of the first and second kind respectively, $J_p(x)$ is the Bessel function of the first kind, with argument $x$ and of order $p$, and $K_j = \omega/\beta_j$ is the wave number in the $j$th layer, while $K = \omega/\beta$ is the wave number in the free-field region. The above functions satisfy the conditions (i) through (iii), and so the equations (2.3.4) and (2.3.5) represent the $(N+1)$th order expansions of $u_z^{fj}$ and $u_z^R$ in terms of Bessel and Hankel functions. It is obvious that other functions could have been selected, but in this work the cylindrical Bessel and Hankel functions are introduced for physically intuitive reasons.

### 2.2.1 Displacement amplitudes

Throughout the numerical analysis, all the variables have been presented in the dimensionless form. For that purpose, the wave numbers $K_j$ and the rigidities $\mu_j$, $j = 1, 2, \ldots, NL$, are normalized with respect to the corresponding parameters of the half-space layer, i.e., $K$ and $\mu$. The distances are normalized with respect to the half-width of the first layer, $a_1$.

For the incident plane $SH$-wave with amplitude 1, the resulting motion can be characterized by the modulus of the displacement amplitude:

$$\text{displ. amplitude} \equiv |u_z| \equiv \{[Re(u_z)]^2 + [Im(u_z)]^2\}^{1/2} \qquad (2.3.12)$$

In the absence of the layered medium, the modulus of ground displacement in uniform half-space is equal to 2.

The displacement in equation (2.3.12) depends on the angle of incidence of $SH$-waves, $\gamma$, and their frequency $\omega$, on the shear wave velocities $\beta$ and $\beta_j$, $j = 1, 2, \ldots, NL$, on

the dimensions and geometry of the layers and the rigidities of the half-space layer and the other layers, $\mu$ and $\mu_j$, $j = 1, 2, \ldots, NL$. Three of these can be combined into one parameter $Ka_1$ given by

$$Ka_1 = \frac{\omega a_1}{\beta} \qquad (2.3.13)$$

which is also equal to

$$Ka_1 = \frac{2\pi a_1}{\lambda} \qquad (2.3.14)$$

where $\lambda = \beta T$ is the wavelength of incident waves with period $T = 2\pi/\omega$. Defining the dimensionless parameter:

$$\eta = \frac{2a_1}{\lambda} \qquad (2.3.15)$$

$Ka_1$ becomes $\pi\eta$. As seen from equation (2.3.15), $\eta$ is the ratio of the total width of the first layer and the wavelength of incident waves, but it can also be thought of as the dimensionless frequency, since $\eta = \omega a_1/\pi\beta$, or a dimensionless wave number, since $\eta = Ka_1/\pi$.

### 2.3 Comparison with known solutions

The above approximate method has been applied to solve two cases with known exact solutions, semi-cylindrical and semi-elliptical alluvial valleys (Trifunac[11]; Wong and Trifunac[6,12]), to test the accuracy of the approximation.

In the case of a semi-cylindrical alluvial valley, a single layer model with a circular boundary was used. The agreement of the surface displacements with those given by Trifunac[11], for a wide range of frequency ($\eta = 0.25$ to $\eta = 2.0$), was found to be excellent.

For the semi-elliptical alluvial valleys, Wong and Trifunac[6,12] give the solution with series involving Mathieu functions. Using the proposed method in this work two families of semi-elliptical alluvial valleys have been analysed: (a) shallow valleys with minor-to-major axis ratios $R = 0.7$ and 0.3 and (b) deep valleys with $R = 0.7$ and 0.5. The model used in this case is the single layer model with boundary of semi-elliptical shape (Fig. 3).

Fig. 4 illustrates an example of surface displacement amplitudes versus normalized distance $x/a_1$ for shallow elliptical alluvial valley with $R = 0.7$ (Fig. 3a), incident angle $\gamma = 0°$, and $\eta = 1.0$. Comparison with exact solution (represented by circles) given by Wong and Trifunac[6,12] indicates excellent agreement. For $\eta = 1.0$, the results were obtained with 12 terms in the series of equation (2.3.6). The number of terms used in these series were 16 for $\eta = 1.5$. The number of points employed on the boundary to apply the boundary conditions was 39. For a deep elliptical alluvial valley with $R = 0.7$ (Fig. 3c) and for incident angle $\gamma = 0°$, and $\eta = 1.0$, the comparison of surface displacement amplitudes is illustrated in Fig. 5.

Moeen-Vaziri and Trifunac[1] present detailed comparison between the exact (Wong and Trifunac[6,12]) and approximate methods of solution for all cases in Fig. 3a through 3d. They also show the effects of varying the number of points along the interfaces $S_j$, where boundary conditions are employed to construct equations (2.3.7), and investigate the required number of
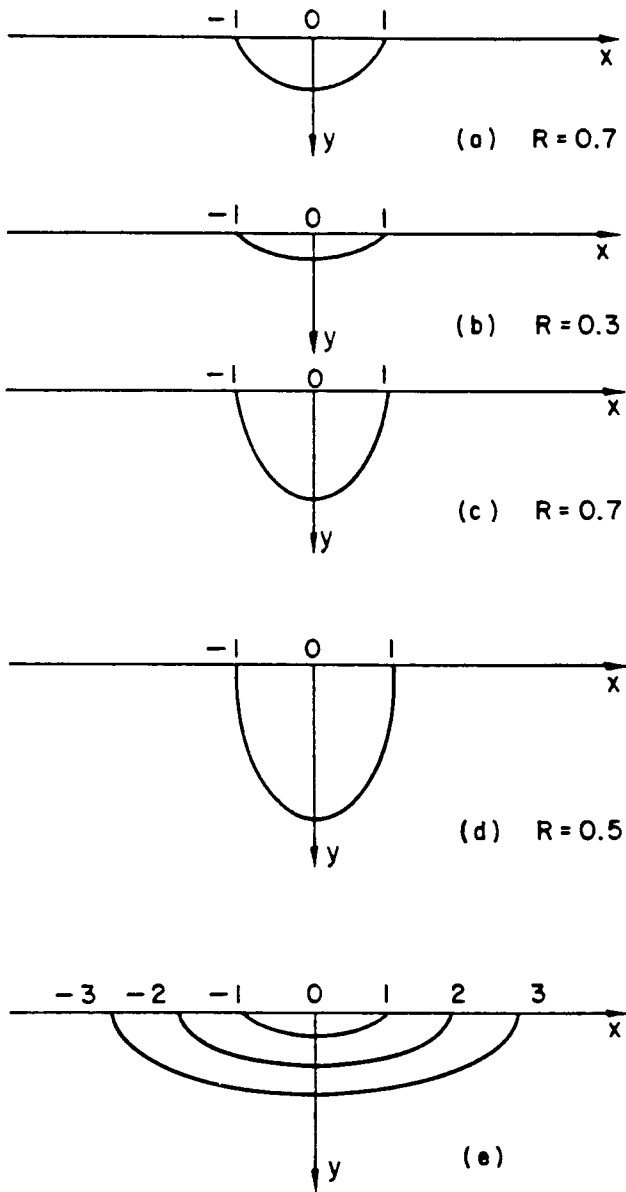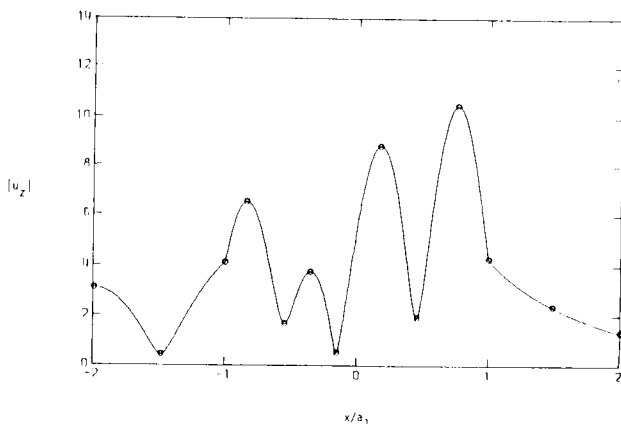
Fig. 3. Models used for comparison of the results

terms in the series representation of $u_z$. They further present a comparison with other proposed methods of solution using the source method and more layers as shown for example in Fig. 3e. Detailed review of their results is beyond the scope of this paper.

### 2.4 An application to practical geometries

Attention is next turned to a more 'realistic' model to study the effects of subsurface inhomogeneities on SH wave amplitudes in strong ground motion. An idealized cross section motivated by the known depth of sediments in the Los Angeles basin was selected for the study. Fig. 6 (after Yerkes et al.[21]) shows the variations of the depth of sediments in the vicinity of Los Angeles. The depth to the basement rock, as determined by oil drillings, varies from zero to over 30 000 feet. The cross section assumed for this illustration (solid line in Fig. 7) has been motivated by the
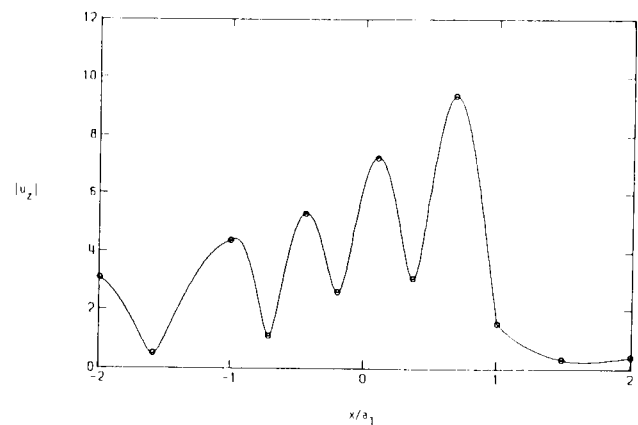


Fig. 5. Surface displacement amplitude for a deep semi-elliptical alluvial valley for incident plane SH-waves, exact solution – dotted circles; approximate solution – solid line ($\eta = 1.0$, $\gamma = 0°$, $K_1/K = 2.0$, $\mu_1/\mu = 0.167$, $R = 0.7$)



Fig. 4. Surface displacement amplitude for a shallow semi-elliptical alluvial valley for incident plane SH-waves, exact solution – dotted circles; approximate solution – solid line ($\eta = 1.0$, $\gamma = 0°$, $K_1/K = 2.0$, $\mu_1/\mu = 0.167$, $R = 0.7$)
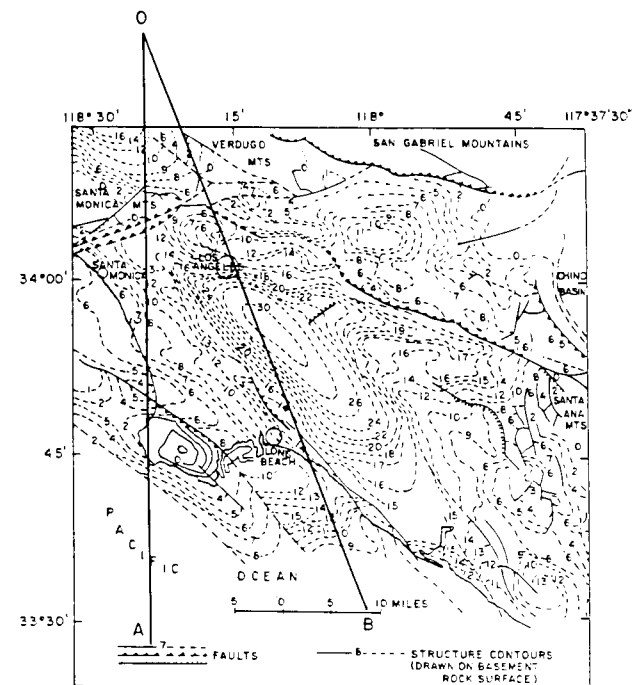


Fig. 6. Thickness of alluvium in the vicinity of Los Angeles (after Yerkes et al.[21])
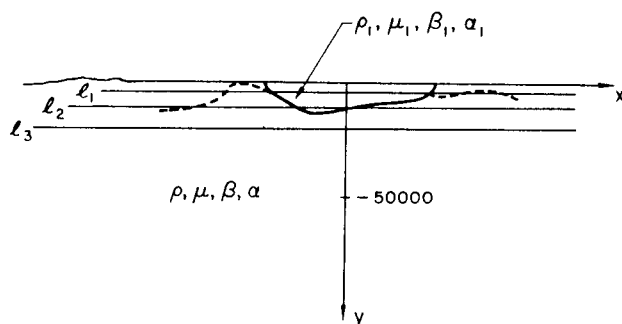
Fig. 7. *Typical simplified cross-section (solid line) of sediments in the Los Angeles basin along profile 0A, and buried horizontal lines $l_1$, $l_2$ and $l_3$. Dashed lines indicate actual depth of sediments*
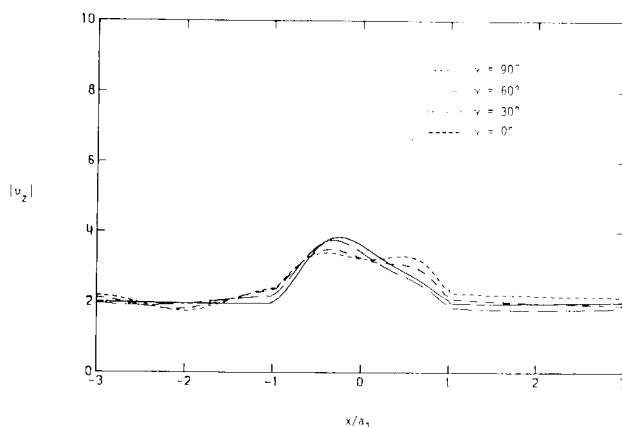


Fig. 8. *Surface displacement amplitudes for cross-section of profile 0A for incident plane SH-waves ($\eta = 0.5$, $K_1/K = 2.3$, $\mu_1\mu = 0.144$)*

section 0A, (dashed line in Fig. 7) of Fig. 6. For the sample calculations the shear-wave velocities of the alluvium layer and the half-space were assumed to be 2.0 km/sec and 4.6 km/sec respectively. The material densities of these two media were assumed to be 2.25 gm/cc and 2.9 gm/cc respectively. The values of the normalized wave number and rigidity are then given by $K_1/K = 2.3$ and $\mu_1/\mu = 0.144$.

### 2.4.1 Surface displacement amplitudes

The results computed for the assumed cross section (solid line in Fig. 7) are given in Figs 8 and 9 and show the amplitudes of surface displacement due to harmonic incident SH-wave of unit amplitude plotted against the dimensionless distance $x/a_1$. These plots are given for two values of dimensionless frequency $\eta$, namely $\eta = 0.5$, and 2.0. Four angles of incidence $\gamma = 90°$, $60°$, $30°$ and $0°$ are considered. The case $\gamma = 0°$ corresponds to a horizontally incident wave travelling from left to right. These figures show that the overall trends of amplification pattern are dependent on the angle of incidence of plane SH-waves, and on the dimensionless frequency. When the wavelength of the incident motion is less than, or comparable to, the dimensions of the inhomogeneity, i.e., when $\eta$ is large, the effects of subsurface inhomogeneity are much more prominent. This result is analogous to the intuitive physical expectation that the waves with long wavelengths do not 'feel' small irregularities in the ground, whereas the waves with short wavelengths do.

The amplitudes vary rapidly from point to point for these short wavelengths, and at some locations, the amplitudes five times the input occur (e.g. Fig. 9). At other points the motion is almost zero. The vibration in these locations can be characterized by nearly-standing waves. The large amplifications and the reductions of the surface displacements result from the focusing of waves reflected through the inhomogeneity.

Moeen-Vaziri and Trifunac[1] present other examples involving different idealized cross-sections of the Los Angles sedimentary basin, to show how the surface and subsurface displacement amplitudes vary with the shape of the sedimentary layer. They also discuss the number of terms in the solution series, as well as the number of boundary points on $S_j$, which were required to compute the ground motion amplitudes.

### 2.4.2 Displacement amplitudes along buried horizontal lines

Next the displacement amplitudes along three buried horizontal lines for the cross section studied above (Fig. 7) are presented. The buried lines $l_1$, $l_2$ and $l_3$ are located at the depths $d = a_1/8$, $d = a_1/4$ and $d = a_1/2$ from the surface, with $a_1$ being the half-width of the inhomogeneity. The results are illustrated for the dimensionless frequencies $\eta = 0.5$ and 2.0 and for the angle of incidence $\gamma = 90°$.

For the cross-section 0A (Fig. 7) the buried line $l_1$ intersects the boundary of the inhomogeneity at $x/a_1 = -0.95$ and $x/a_1 = +1.0$. The corresponding intersection points for line $l_2$ are at $x/a_1 = -0.74$ and $x/a_1 = +0.33$. The buried line $l_3$ does not intersect the boundary of the inhomogeneity (Fig. 7).

Figs 10 and 11 present the displacement amplitudes along these three buried lines versus dimensionless distance $x/a_1$ for the cross-section in Fig.7. Additional plots of such displacement amplitudes, for other cross-sections in the Los Angeles basin have been presented by Moeen-Vaziri and Trifunac[1]. The results they discuss are for four angles of incidence $\gamma = 90°$, $60°$, $30°$ and $0°$ and four values of the dimensionless frequency $\eta = 0.5$, 1.0, 1.5 and 2.0. As the depth of the buried line increases, the influence of the inhomogeneity decreases. For small values of $\eta$, long wavelengths, the influence of the subsurface irregularity almost disappears. For higher values of $\eta$, short wavelengths, the rapid change of the
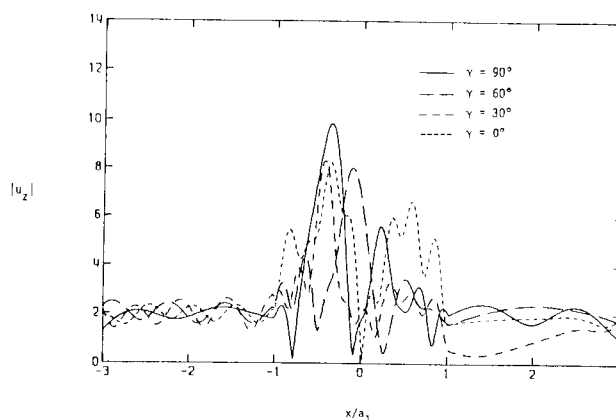


Fig. 9. *Surface displacement amplitudes for cross-section of profile 0A for incident plane SH-waves ($\eta = 2.0$, $K_1/K = 2.3$, $\mu_1/\mu = 0.144$)*
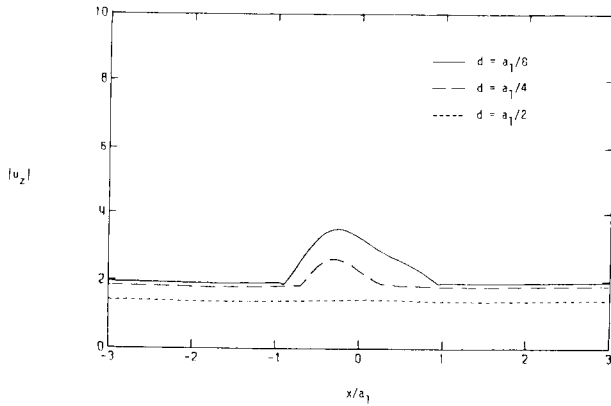
*Fig. 10. Displacements amplitudes along three buried horizontal lines for cross-section of profile 0A for incident plane SH-waves ($\gamma = 90°$, $\eta = 0.5$, $K_1/K = 2.3$, $\mu_1/\mu = 0.144$)*



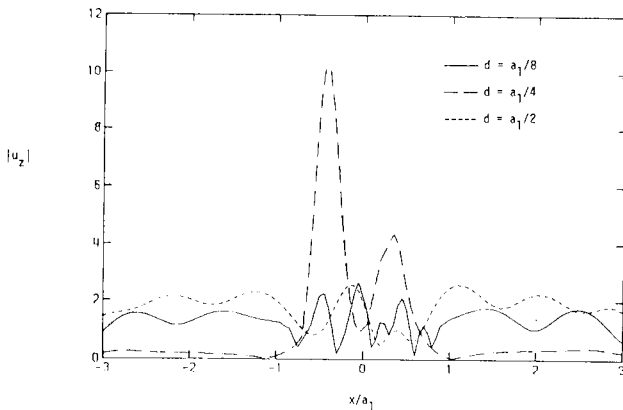*Fig. 11. Displacement amplitudes along three buried horizontal lines for cross-section of profile 0A for incident plane SH-waves ($\gamma = 90°$, $\eta = 2.0$, $K_1/K = 2.3$, $\mu_1/\mu = 0.144$)*

amplitudes from point to point along the lines closer to the surface ($l_2$ and $l_1$) can still be seen. Fig. 11 illustrates an interesting case showing that the motions at depth ($d = a_1/4$) can be larger than the motions on the surface.

### 2.4.3 Surface displacement amplitudes for a three layer model

For a small portion along the section 0B, Fig. 6, a three layer model for the Los Angeles area is assumed for the following example (Yerkes *et al.*[21] and Gutenberg[22]). This model is shown in Fig. 12. The shear wave velocities in the layers of the inhomogeneous model are chosen to be $\beta_1 = 1.4$ km/sec, $\beta_2 = 2.6$ km/sec and $\beta_3 = 3.8$ km/sec respectively. The material densities of these layers are assumed to be $\rho_1 = 2.1$ gm/cc, $\rho_2 = 2.4$ gm/cc and $\rho_3 = 2.7$ gm/cc respectively. The shear wave velocity and the material density of the half space are $\beta = 4.6$ km/sec and $\rho = 2.9$ gm/cc, as before. With these assumed shear wave velocities and the material densities, the values of the normalized wave numbers become $K_1/K = 3.28$, $K_2/K = 1.77$ and $K_3/K = 1.21$. The values of the normalized rigidity factors are then: $\mu_1/\mu = 0.065$, $\mu_2/\mu = 0.257$ and $\mu_3/\mu = 0.625$.

Figs 13 through 16 present the surface displacement amplitudes versus normalized distance $x/a_1$ for the model shown in Fig. 12. Four values of dimensionless frequency $\eta$ are considered, $\eta = 0.5$, 1.0, 1.5 and 2.0. The results are

given for four angles of incidence $\gamma = 90°$, $60°$, $30°$ and $0°$. It can be seen that the patterns of amplification for this case are more complicated than for a single layer model. The complexity of these amplitudes increases as the value of the dimensionless frequency $\eta$ increases. In this case, the amplifications almost seven times the input amplitude occur at some locations along the surface.

### 2.4.4 Displacement amplitudes for transient excitation

Effects of the subsurface inhomogeneities upon the transient earthquake motions can be studied by Fourier analysis and synthesis, by using the above results in the frequency domain. In this framework, the results
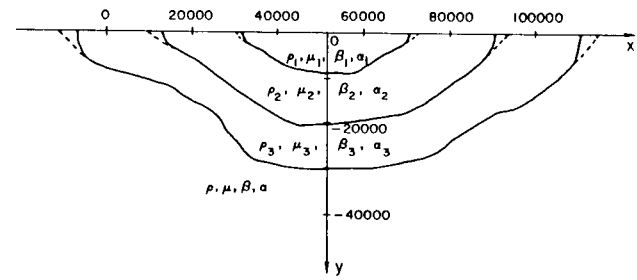


*Fig. 12. A three-layer model along a small portion of profile 0B of Los Angeles basin*
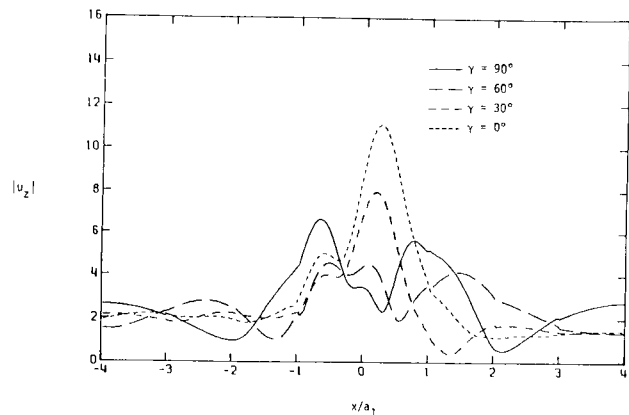


*Fig. 13. Surface displacement amplitudes for a three-layer model along profile 0B for incident plane SH-waves ($\eta = 0.5$, $K_1/K = 3.28$. $K_2/K = 1.77$, $K_3/K = 1.21$, $\mu_1/\mu = 0.065$, $\mu_2/\mu = 0.257$, $\mu_3/\mu = 0.625$)*
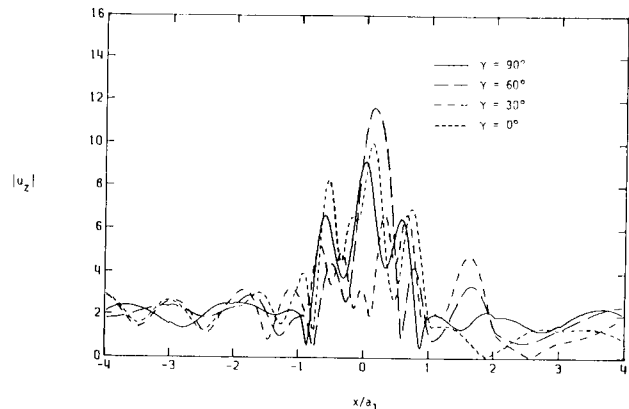


*Fig. 14 Surface displacement amplitudes for a three-layer model along profile 0B for incident plane SH-waves ($\eta = 1.0$, $K_1/K = 3.28$, $K_2/K = 1.77$, $K_3/K = 1.21$, $\mu_1/\mu = 0.065$, $\mu_2/\mu = 0.257$, $\mu_3/\mu = 0.625$)*
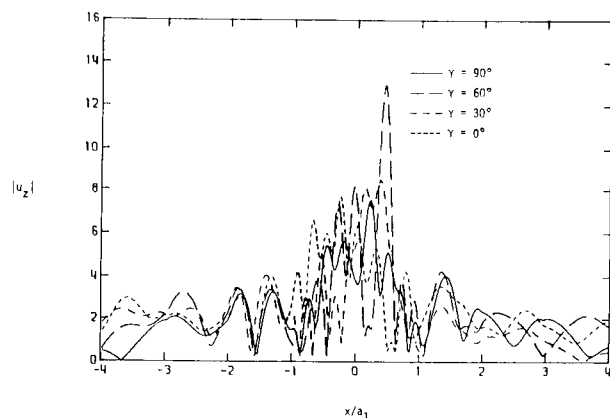
*Fig. 15. Surface displacement amplitudes for a three-layer model along profile OB for incident plane SH-waves ($\eta = 1.5$, $K_1/K = 3.28$, $K_2/K = 1.77$, $K_3/K = 1.21$, $\mu_1/\mu = 0.065$, $\mu_2/\mu = 0.257$, $\mu_3/\mu = 0.625$)*
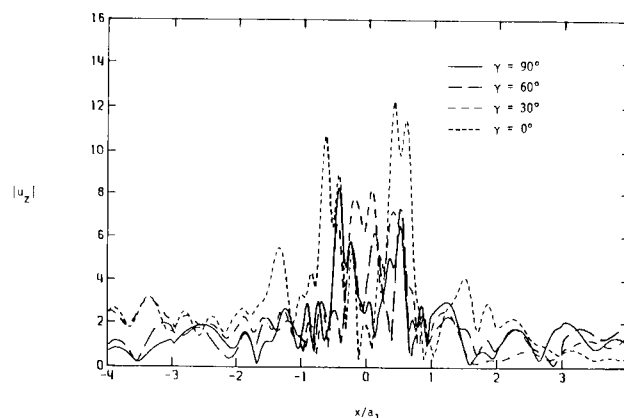


*Fig. 16. Surface displacement amplitudes for a three-layer model along profile OB for incident plane SH-waves ($\eta = 2.0$, $K_1/K = 3.28$, $K_2/K = 1.77$, $K_3 K = 1.21$, $\mu_1/ = 0.065$, $\mu_2/\mu = 0.257$, $\mu_3/\mu = 0.625$)*

presented in this paper represent transfer functions, which can be used to modify the Fourier transform of incident *SH* waves and, through Fourier synthesis, give the transient earthquake motions at any location in the model. Detailed discussion of such transient motions is beyond the scope of this paper, as it depends on numerous parameters which describe the incident motion, and is perhaps better suited for a specific case study. The reader may find some simplified examples of such transient analyses in the report by Moeen-Vaziri and Trifunac[1].

## CONCLUSIONS

The results of this study can be summarized as follows:

1. The wave expansion representation of the scattered and diffracted fields of plane *SH*-waves near and inside two-dimensional inhomogeneities is capable of representing the strong ground motion there for long incident waves. The method has been tested for $\eta \leqslant 2$ (where $\eta$ is the ratio of the size of the inhomogeneity to the wave length of incident waves). We found that our results agree favourably with exact series solutions of semi-elliptical inhomogeneities.

2. The transient earthquake excitation, represented by its Fourier transform, can be combined with the results of this study, representing the complex transient functions of the response in or near inhomogeneity, to compute transient strong ground motion at any point in the medium. It is assumed, of course, that the medium responds linearly, for all amplitudes of excitation. This, however, does not seem to result in any significant limitations since, for the majority of applied earthquake engineering applications, response of alluvium and soil does remain in the linear response range.

3. Extension of the results presented here to shorter wave lengths ($\eta > 2$) is straightforward from the formal point of view. The more advanced approach is required, however, in the inversion of the resulting least-squares equation, since this inversion becomes progressively unstable with the size of the resulting matrices.

## REFERENCES

1 Moeen-Vaziri, N. and Trifunac, M. D. Investigation of Scattering and Diffraction of Plane Seismic Waves through Two-Dimensional Inhomogeneities, Report No. 86-03, Dept. of Civil Eng., Univ. of Southern California, Los Angeles, California, 1986

2 Trifunac, M. D. Scattering of Plane SH Waves by a Semi-Cylindrical Canyon, *Earthquake Eng. and Struct. Dyn.*, 1973, **1**, 267–281

3 Sabina, F. J. and Willis, J. R. Scattering of SH-Waves by a Rough Half-Space of Arbitrary Shape, *Geophysical Journal*, 1975, **42**, 685–703

4 England, R., Sabina, F. J. and Herrera, I. Scattering of SH-Waves by Superficial Cavities of Arbitrary Shape using Boundary Methods, *Comunicaciones Técnicas*, 1978, Vol. 9

5 Sills, L. B. Scattering of Horizontally Polarized Shear Waves by Surface Irregularities, *Geoph. J.R. Astr. Soc.*, 1978, **54**, 319–348

6 Wong, H. L. and Trifunac, M. D. Scattering of Plane SH Waves by a Semi-Elliptical Canyon, *Earthquake Eng. and Struct. Dyn.*, 1974a, **3**, 157–169

7 Sáchez-Sesma, F. J. and Rosenblueth, E. Ground Motion at Canyons of Arbitrary Shape under Incident SH-Waves, *Earthquake Eng. and Struct. Dyn.*, 1979, **7**, 441–450

8 Wong, H. L., Trifunac, M. D. and Westermo, B. Effects of Surface and Subsurface Irregularities on the Amplitudes of Monochromatic Waves, *Bull. Seism. Soc. Amer.*, 1977, **67**, 353–368

9 Sánchez-Sesma, F. J., Herrera, I. and Avilés, J. A Boundary Method for Elastic Wave Diffraction: Application to Scattering of SH-Waves by Surface Irregularities, *Bull. Seism. Cos. Amer.*, 1982, **72**, 473–490

10 Wong, H. L. and Jennings, P. C. Effects of Canyon Topography on Strong Ground Motion, *Bull. Seism. Soc. Amer.*, 1975, **65**, 1239–1257

11 Trifunac, M. D. Surface Motion of a Semi-Cylindrical Alluvial Valley for Incident Plane SH Waves, *Bull. Seism. Soc. Amer.*, 1971, **61**, 1755–1770

12 Wong, H. L. and Trifunac, M. D. Surface Motion of a Semi-Elliptical Alluvial Valley for Incident Plane SH Waves, *Bull. Seism. Soc. Amer.*, 1974b, **64**, 1389–1408

13 Aki, K. and Larner, K. L. Surface Motion of a Layered Medium Having an Irregular Interface due to Incident Plane SH-Waves, *J. Geophys. Res.*, 1970, **75**, 933–954

14 Bard, P. Y. and Bouchon, M. The Seismic Response of Sediment-Filled Valleys, Part 1, The Case of Incident SH-Waves, *Bull. Seis. Soc. Amer.*, 1980, **70**, 1263–1286

15 Sánchez-Sesma, F. J. and Esquivel, J. A. Ground Motion on Alluvial Valleys under the Incident Plane SH-Waves, *Bull. Seism. Soc. Amer.*, 1979, **69**, 1107–1129

16 Lee, V. W. and Trifunanc, M. D. Stresses and Deformations near Circular Underground Tunnels Subjected to Incident SH-Waves, *ASCE, EMD*, 1979, **105**, 643–659

17    Moeen-Vaziri, N. and Trifunac, M. D. A Note on the Vibrations
      of a Semi-Circular Canal Excited by Plane SH-Wave, *Bull. ISET*,
      1981, **18**, 88–100
18    Moeen-Vaziri, N. and Trifunac, M. D. Scattering of Plane SH-
      Waves by Cylindrical Canals of Arbitrary Shape, *Int. J. Soil Dyn.
      and Earthquake Eng.*, 1984, **4**, 18–23
19    Sáchez-Sesma, F. J. Diffraction of Elastic Waves by Three-
      Dimensional Surface Irregularities, *Bull. Seism. Soc. Amer.*, 1983,
      **74**

20    Pao, Y. H. and Mow, C. C. Diffraction of Elastic Waves and
      Dynamic Stress Concentrations, Crane, Russak and Company
      Inc., New York, 1973
21    Yerkes, R. F. McCulloh, Schoellhamer, J. E. and Vedder, J. G.
      Geology of the Los Angeles Basin, California – an Introduction,
      US Geological Survey Professional Paper 420-A, 1965
22    Gutenberg, B. Effects of Ground on Earthquake Motion, *Bull.
      Seism. Soc. Amer.*, 1957, **47**, 221–250